SPE 115929

Modeling Leakage through Faults of CO_2 Stored in an Aquifer

Kyung Won Chang,* Susan E. Minkoff,** and Steven L. Bryant,* SPE
*The University of Texas at Austin
**The University of Maryland, Baltimore County

This paper was prepared for presentation at the 2008 SPE Annual Technical Conference and Exhibition held in Denver, Colorado, USA, 21–24 September 2008.

Abstract

For secure storage of CO_2 within geologic formations, the integrity of caps – overlying strata that are impervious to CO_2 – is an important factor. Geologic structures, notably faults and the damage zones surrounding them may provide a conduit for CO_2 to escape through a cap. If the fault encounters shallower permeable formations, the CO_2 rising along the fault can enter them. This lateral migration would attenuate the rate at which CO_2 enters sensitive formations such as aquifers used for drinking water. Thus, CO_2 leakage along faults will have three behaviors: upward migration from the storage formation along a fault, lateral movement from the fault into permeable layers, and a continued but attenuated CO_2 flux along the fault above the layers.

Here we develop a quasi-1D single-phase flow model for these three behaviors. The model is highly simplified and intended to be suitable for inclusion in a certification framework for geologic storage projects. The model accounts for flow from the fault into a permeable formation using a leakoff coefficient. The coefficient can vary spatially and depends on the geometry and petrophysical properties of the formation. We apply a commercial simulator to verify the quasi-1D model. A series of examples illustrates the controlling mechanisms for leakage rate from the reservoir and its attenuation by flux into shallower layers.

Nonlinearities arise even in this simple model. For example, leakage flux and the degree of attenuation vary nonlinearly with the permeability of the fault and the permeability of the shallower layer(s) intersected by the fault. Layers nearest the CO_2 storage formation produce the most attenuation. But the percentage of CO_2 entering overlying formations from the fault varies linearly with the ratio of fault permeability to leakoff coefficient. A simple estimate of the leak-off coefficient compares favorably with 2D, full-physics simulations. If the permeable layer is dipping, CO_2 enters it asymmetrically and estimating the leakoff coefficient is less straightforward. The difference arises because of preferential flow within the layer (CO_2 in the upper part, water below).

Introduction

If society elects to reduce anthropogenic emissions of CO_2, geologic storage will be one of the key technologies for achieving this goal. In the standard approach to storage, CO_2 is captured from fixed sources such as coal-fired power plants, compressed and injected at supercritical conditions into a suitable target formation. For typical geothermal gradients, suitable formations are found at depths of 800 m (2600 ft) or more, as their temperatures and pressures will be above the critical point of CO_2. Trapping the injected CO_2 involves one or more mechanisms (Bachu *et al.* 1994; IPCC 2006): (1) permeability trapping by an impervious confining layer or cap rock; (2) solubility trapping by CO_2 dissolution into the aqueous phase in the pore space; (3) mineralogic trapping by chemical reaction of cations with dissolved CO_2 to precipitate carbonate minerals; (4) residual phase trapping as the nonwetting CO_2 phase becomes disconnected in pores or small clusters of pores; (5) stratigraphic trapping below a formation whose capillary entry pressure is greater than the capillary pressure of the CO_2 phase. An intact confining layer is necessary for several trapping mechanisms. However, sedimentary basins often contain geological discontinuities which are potential pathways for leakage through the confining layer. Faults are one such discontinuity and are prevalent in many regions where CO_2 storage is likely to be implemented. Wells are a man-made discontinuity, likewise prevalent in likely storage regions. We do not treat them here, but the conceptual model for faults provides a foundation for assessing leakage along wells (Huerta *et al.* 2008).

It is therefore important to examine the consequences if injected CO_2 encounters a fault. Figure 1 illustrates the situation of interest. A conductive fault can be a major pathway for the CO_2 plume due to its large transfer capacity. However CO_2 leaking

from the main target formation does not necessarily reach the Earth's surface. It may not even reach shallower formations of economic interest (mines, hydrocarbon reservoirs, aquifers that serve as underground sources of drinking water (USDW)). Instead, the rising CO_2 can be secondarily trapped by shallow subsurface structures, dissolution and residual phase creation (Lindeberg 1997). It can also migrate into permeable formations encountered by the conductive fault. On one hand, this migration attenuates the upward flux. On the other, it spreads the influence of the CO_2 across a wider area. The near-surface zone can also attenuate CO_2 leaks and decrease CO_2 concentration reaching the surface. The attenuation rate is sensitive to the subsurface properties (Oldenburg and Unger 2003). Thus, the effect of a conductive fault on net CO_2 storage needs to be analyzed based on the geometric and petrophysical properties of the formation, of the fault and of the overlying permeable layer, and on the boundary conditions (pressure in the storage formation and in the overlying layers).

The physics of a CO_2 plume rising long vertical distances through the Earth's crust can be complex (Pruess 2003). Here we present a highly simplified model, motivated by two considerations. One is geological: in many sedimentary basins, a fault is unlikely to be conductive continuously from depth to the shallow subsurface. Leakage to surface or to USDW will involve a sequence of upward (along a fault) and lateral (within a permeable layer) migrations. Thus we will consider moderate conduit lengths of 1000 meters or less. The other consideration is practical: for CO_2 storage to be implemented broadly and rapidly enough to mitigate anthropogenic emissions, thousands of storage projects will be needed. Each will have to be permitted by regulators in a streamlined yet robust and transparent way. Unfortunately the physical properties of most storage formations – deep saline aquifers – will be poorly constrained prior to injection. In light of this uncertainty, simple models that allow adequate physics-based risk assessment will be valuable tools for operators, regulators and policymakers.

The model presented here was developed to be applicable within the Certification Framework (CF) for geologic storage (Oldenburg and Bryant 2007, Oldenburg *et al*. 2008). The purpose of the CF is to provide a framework for project proponents, regulators, and the public to analyze the risks of geologic CO_2 storage in a simple and transparent way. The risk analysis would be performed to certify the startup and decommissioning of sites for geologic CO_2 storage. The CF currently emphasizes risks associated with subsurface processes and excludes compression, transportation, and injection-well leakage risk. The CF is designed to be simple by (1) using proxy concentrations or fluxes, rather than complicated exposure functions, for quantifying impact; (2) using a catalog of pre-computed CO_2 injection results (Kumar 2008), and (3) using a simple framework for calculating leakage risk. For transparency, the CF endeavors to be clear and precise in terminology in order to communicate to the full spectrum of stakeholders. One concept of the CF is that leakage occurs along conduits from the storage volume to "compartments" such as hydrocarbon reservoirs or USDW. The risk associated with leakage is the product of the probability of leakage and the impact of that leakage. The flux of CO_2 contributes to impact. Thus the goal of the fault-leakage model is to estimate flux at an "outlet" of a conductive fault, once CO_2 has arrived at the "inlet".

The overarching criteria of the CF and the models within it are simplicity, transparency and acceptability. Here we emphasize the requirement of simplicity. The subsurface data available as input to any numerical model in the CF will always be limited. This limitation is especially troublesome in the case of injection into saline aquifers. Saline aquifers provide large storage capacity but are not well characterized due to the small number of existing wells which could provide geologic information about that particular region of the subsurface. The flow properties of faults are even more uncertain, at least before injection begins. In principle the required properties could be obtained from appropriate measurement campaigns. In practice, measurement will increase the cost of storage, and cost minimization will be a high priority for any greenhouse gas mitigation strategy. Moreover, the most reliable measurements would come from wells drilled into the formation or through the fault. These wells would themselves be potential pathways for leakage. The philosophy of the fault-leakage model is thus to identify the key physical phenomena controlling leakage flux. The sensitivity of the flux to physical parameters provides insight as to which aquifer properties should be measured when designing or monitoring a storage project.

In subsequent sections we present a quasi-1D mathematical description of CO_2 flux using the "leaky conduit" model. The leaks correspond to permeable formations intersected by the conduit. A "leakoff coefficient" is used to control the rate of leakage. We describe a method for estimating these coefficients from the properties of the formations. To test whether these idealizations are reasonable, we carry out simulations of the full physics of the problem in a 2D domain.

Quasi-1D Modeling Approach

Assumptions. We assume that the CO_2 storage reservoir is located at sufficient depth for the carbon dioxide to be modeled as a slightly compressible fluid. Intersecting this storage volume is a fault, either vertical or at a fixed angle to the storage reservoir (Fig. 1). The most stringent assumption of the model is that we only consider the flow of a single fluid, namely CO_2, along the fault. Leakage of CO_2 from saline aquifers will involve cocurrent and countercurrent flow of two fluid phases (brine and carbon dioxide), and relative permeability and capillary pressure play critical roles in buoyancy driven flow (e.g. Lakshminarasimhan *et al*. (2006) and Saadatpoor *et al*. (2008)). However, for the purposes of quantifying leakage mechanisms, single phase flow of CO_2 (Darcy's law) is assumed to capture the relationship between flux and driving force. We test this idealization later in this paper via two-phase flow simulations carried out using the GEM commercial simulator (Nghiem *et al*. 2006).

We treat the fault as a one-dimensional conduit with spatially varying permeability. Thus the complexities of the fault core and the damage zone surrounding it are averaged into a single array of permeability values. This simplification is extreme but it is consistent with concepts such as the shale gouge ratio (Yielding *et al*. 1997). Permeability in the direction of the fault throw is likely to be small in regions where sufficient shale is entrained in the fault. The existence of such a region will control CO_2 flux along the fault. This is true even in a long fault that elsewhere juxtaposes sand against sand and is very conductive.

Accounting for permeability variation along the fault will be important in estimating the risks associated with faults for a geologic storage project.

We further assume that the CO_2 remains slightly compressible as it rises along the fault. If the CO_2 moves slowly enough to equilibrate with the pressure and temperature of the surrounding formations, slight compressibility is a reasonable assumption for two situations. One is for deep leaks, those along faults beginning and ending at depths greater than about 1200 m (3500 ft). The other situation is shallow leaks, along faults less than 600 m (2000 ft) in depth. The density of CO_2 for hydrostatic pressure gradient and a representative geothermal gradient (29.2°C/1 km or 1.6°F/100 ft, $T_{surface}$ = 15°C or 59°F) is shown as a function of depth in Fig. 2a. The combined variation of pressure and temperature yields an almost linear variation of CO_2 density with depth for D > 3500 ft and for D < 2000 ft. The variation in each region can be approximated well with a slightly compressible model with constant compressibility (Table 1). Leaks which rise through intermediate depths, 2000 ft < D < 3500 ft, could also be approximated with a slightly compressible model, and long leakage paths could be modeled by piecing together the appropriate behavior. We do not explore that possibility here. All results are for a single value of compressibility. For simplicity we assume constant viscosity. Figure 2b shows that this is a reasonable assumption if we take a value around 0.000018 Pa-s (0.018 cp) in the "shallow leak" region and 0.00006 Pa-s (0.06 cp) in the "deep leak" region, respectively. This simplification of the phase behavior also assumes that the pressure-temperature profile does not cross the gas/liquid phase boundary. As indicated in Fig. 2c, this assumption is valid for typical geothermal gradients and surface temperatures.

The model is "quasi"-1D because CO_2 is allowed to enter neighboring strata lateral to the fault (Fig. 3), but flow in these lateral formations is not explicitly modeled. Because we represent the fault as a "leaky conduit", we refer to flow into these strata as "leakage". The connotation of "leakage," that is, flow from the fault vs. flow from the storage formation, should be clear from the context. We will also use the term "attenuation" to indicate CO_2 leaving the fault and entering a permeable layer. We model leakage from the fault via a specially designed source term. The lateral formations may be horizontal or inclined. The angle of inclination adds buoyancy to the driving force for leakage into the lateral formation.

We assume that the fault contains water initially (implemented by assuming the initial pressure along the fault is hydrostatic). The top of the fault is assumed to be at hydrostatic pressure. The bottom boundary of the fault is set to a pressure above hydrostatic. The value of this over-pressurization is proportional to the height of the column of stored CO_2. The pressure in the CO_2 phase is taken to be hydrostatic at the base of the column. The thicker the column, the higher the pressure in the CO_2 at the location where the fault intersects the storage formation. This high pressure at the bottom of the fault (along with buoyancy) is the driving force for flow along the fault.

Mathematical Model. The single-phase flow equation derived from conservation of mass and Darcy's law is given by Ewing (1983):

$$\frac{\partial}{\partial t}(\phi\rho) = \nabla \cdot \frac{\rho k}{\mu}(\nabla p - \rho g \nabla D) + q \tag{1}$$

where ϕ is porosity, ρ is fluid density, p is pore pressure, k is vertical permeability of the fault, μ is fluid viscosity, g is the gravitational constant, D is the depth vector, and q denotes the source or sink term.

Mathematically, the boundary and initial conditions described in the previous subsection are modeled as follows. If p_z denotes hydrostatic pressure then our initial condition along the fault at initial time t_0 is $p(z,t_0) = p_z(z)$. The pressure at the top of the fault is given by $p(z_{top}, t) = p_z(z_{top})$, and the pressure at the bottom of the fault is $p(z_{bottom}, t) = p_z(z_{bottom}) + X$ where X is an additional pressure due to the CO_2 storage compartment below the fault. Finally the source term is modeled by a vector of "leakoff coefficients" q_{leak} times a potential difference. The coefficients and the potential difference vary along the fault. Physically these leakoff values are only nonzero at depths z corresponding to leaks from the fault into lateral strata. The leakage source term is, therefore, described by

$$q(z,t) = q_{leak}(z)\left[p(z,t) - p_z(z) - \rho(z)\, g \sin\gamma\right] \tag{2}$$

Here in the gravity term, the gradient of the depth vector has been evaluated in the direction of the permeable formation. It is zero for horizontal formations and equal to $\sin\gamma$ for formations inclined at angle γ to the horizontal.

Equation 1 is a single equation in two unknowns (density ρ and pressure p). To reduce this equation to one equation in one unknown we make use of the equation of state which relates density to pressure via the differential equation (Chen *et al*. 2006):

$$\frac{\partial\rho}{\partial t} = c_f \rho \frac{\partial p}{\partial t} \tag{3}$$

The end result is that our one-dimensional model requires solution of the following equation for fluid pressure along the fault (Chen *et al*. 2006):

$$\rho\phi c_t \frac{\partial p}{\partial t} = \frac{\partial}{\partial z}\frac{\rho k}{\mu}\left(\frac{\partial p}{\partial z} - \rho\, g\, \sin\theta\right) + q \tag{4}$$

Here the angle θ is the dip angle for the fault measured from horizontal (so a vertical fault has *sin* θ = 1). We have introduced the total compressibility c_t defined by $c_t = c_f + \frac{\phi_0}{\phi} c_r$, where ϕ_0 is a reference porosity at reference pressure p_0, c_f is fluid compressibility, and c_r is rock compressibility. For a slightly compressible fluid we approximate the exponential solution of the equation of state by a linear Taylor series, namely, that

$$\rho \approx \rho_0 \left[1 + c_f \left(p - p_0\right)\right] \tag{5}$$

which then requires solution of a nonlinear flow equation of the form of Eq. 4. The values of c_f for CO_2 in the "shallow leak" and "deep leak" regions are given in Table 1. We solve this system numerically by discretizing the spatial derivatives using Galerkin finite elements and using backward Euler for the time derivative.

Leakoff Coefficients. The leakoff coefficient q_{leak} in the source term can be estimated from the formation and fluid properties. The estimate is based on the Darcy's law and the modeling assumptions described above. Assuming further that flow into the layer is steady, linear and one-dimensional flow, we write

$$Q = \frac{k_r k_{layer} A}{\mu}\left(\frac{\Delta\Psi}{L}\right) \tag{6}$$

where Q is volumetric flow rate of CO_2 (reservoir conditions), k_r is relative permeability, k_{layer} is absolute permeability of the layer into which CO_2 enters, A is cross-sectional area for leakage (i.e. the area of the intersection between fault and layer) and L is the distance between fault and the far boundary of the layer, where the pressure is hydrostatic. The potential difference is given by

$$\Delta\Psi = \left(p_1 - p_2\right) + \left(\rho_1 z_1 - \rho_2 z_2\right) g \sin\gamma \tag{7}$$

Subscripts '1' and '2' define locations; at location '1' the fault intersects the permeable layer and at location '2' the hydrostatic boundary is located. Fig. 4 shows the schematic description. For horizontal layer(s) we have $\gamma = 0$ and the driving force is only the pressure difference between fault and far-field. We neglect the variation in CO_2 density between locations '1' and '2'. To obtain leakoff coefficients, we rewrite Eq. 6 in the form

$$\Phi(z) = \rho(z)\frac{Q(z)}{A} = q_{leak}(z)\Delta\Psi(z) \tag{8}$$

where Φ is the mass flux into the layer and q_{leak} is the leakoff coefficient:

$$\mathrm{q_{leak}} = \frac{\rho(\mathrm{z})\,\mathrm{k_r k_{layer}}}{\mu\,\mathrm{L}} \tag{9}$$

The leakoff coefficient consists of five parameters: CO_2 density, relative permeability and viscosity, permeability of layer, and a distance from a fault to hydrostatic boundary. The absolute permeability of the layer differs in general from the fault permeability at the same depth. The relative permeability is evaluated at the CO_2 saturation at the Buckley-Leverett front. The rationale for this choice is discussed below. The frontal saturation is easily computed graphically from an extension of fractional flow theory that accounts for the mutual solubility of water and CO_2 (Noh *et al*. 2007). The distance L measures the extent of the pressure perturbation within the layer.

Results and Discussion

Quasi-1D Results. In the following section we detail results derived from the one-dimensional fault model. Specifically we describe fundamental mechanisms that can be illustrated with this simple model and which are of interest for assessing leakage of CO_2 from storage sites. In these simulations we consider a 1000 m (3280 ft) long vertical fault extending from a depth of 1000 m (3280 ft) down to 2000 m (6560 ft) into the earth. We will assume in all of the simulations except the last that the CO_2 storage reservoir abuts the bottom of the fault and that the storage compartment is 500 m (1640 ft) thick (resulting in an over-pressurization of 5 MPa (725 psi) at the top of the reservoir (bottom of the fault)). In the final simulation discussed in this section we consider the effect of the pressure value at the bottom of the fault. The reservoir is assumed to have constant CO_2

viscosity of 0.00005 Pa-s, an initial reservoir porosity of 20%, an initial fluid pressure of 18 MPa (2611 psi), and an initial CO_2 density of 647 kg/m^3 (40.39 lb/ft^3),. The rock compressibility is 1×10^{-11} Pa^{-1}. Our mathematical model assumes the fluid is only slightly compressible. This assumption allowed us to replace the exponential relationship between density and pressure by the linear Taylor series approximation (Eq. 5). In Fig. 5 we see that values of fluid compressibility which are smaller than about 1×10^{-9} Pa^{-1} result in small variations in density along a fault at steady state flow conditions. However, when the compressibility reaches values of 5×10^{-9} Pa^{-1} the fluid density varies by about 10% along the length of a 1000 m (3280 ft) long vertical fault. In Fig. 6 we illustrate the effect of compressibility on mass flux. The fault permeability is uniform at 1 D, and we assume there is a single leak along the fault at a depth of 1400-1450 m (4600-4760 ft). The source coefficient q_{leak} at this depth takes the value -1.5×10^{-8} sec/m. (The negative sign ensures that the leakage flux is out of the fault and into the permeable layer.) In Fig. 6 we see that for this leak the effect of compressibility is minor. The main effect of larger values for compressibility (and hence a bigger range of density values) is the time needed to reach steady state. As the value of compressibility increases more time steps are needed to reach a steady state solution.

Having illustrated a range of plausible values for which the small compressibility assumption holds, we now turn to simulations that illustrate fundamental conclusions we can make about leakage. We assume in all simulations that follow that fluid compressibility, c_f is 1×10^{-9} Pa^{-1}. Our first conclusion is that *leaks near the bottom of the fault have a greater impact than leaks which occur at shallower depths.* We again consider a 1000 m (3280 ft) long vertical fault which extends from 1000-2000 m (3280-6560 ft) in depth. CO_2 viscosity, reservoir porosity, rock compressibility, and initial fluid density are all taken to have the same values as those given in the last simulation. The fault permeability is again uniform at 1 D. In these simulations the leakoff coefficient is non-zero along two sections of the fault: namely from 1100-1150 m (3600-3770 ft) and from 1800-1850 m (5900-6070 ft) depth. At these two locations q_{leak} is assigned the value -1.5×10^{-9} sec/m. So the value of the leakoff coefficient is the same at these two leakage depths.

In Fig. 7 we show the steady state mass flux along the fault. Escaping from the storage formation is 0.26 kg CO_2/m^2-s. Most of this flux (about 80%) enters the deeper permeable formation at 1800 m (5900 ft). Relatively little attenuation (about 5% of the escape flux) occurs in the shallower permeable formation. Thus only 15% (0.07 kg CO_2/m^2-s) of the CO_2 escaping the storage formation reaches the top of the fault. In contrast in Fig. 8 we have simulated the same situation but with only the shallow leak. The flux escaping the storage formation is less than half the value with the deeper leak, about 0.12 kg CO_2/m^2-s. This flux undergoes only 30% attenuation into the shallow permeable formation, even though the leakoff coefficient is identical at both depths. Thus the flux of CO_2 at the top of the fault is 0.08 kg CO_2/m^2-s. Although much less CO_2 escapes the storage formation, more CO_2 reaches the top of the fault when the leakage layer is near the top of the fault. This counterintuitive result is the consequence of the decrease in driving force for leakage (CO_2 pressure in fault less hydrostatic water pressure in the formation) as CO_2 rises. From the perspective of risk assessment, the CO_2 reaching the top of the fault is the greatest concern. Thus a corollary of our first conclusion is that *attenuation can reduce risk even if more CO_2 leaves the storage formation.*

A second major conclusion is that *the attenuation is proportional to the ratio of fault permeability to leakoff coefficient (k/q_{leak}).* Figure 9 shows mass flux for a single permeable layer between 1700-1750 m (5580-5740 ft) depth with a leakoff coefficient of -1.5×10^{-8} sec/m. The fault permeability is uniform at 10 D. We see that the flux of CO_2 out the top of the fault is (- 0.75 kg/m^2-s)/(-2.1 kg/m^2-s) or approximately 0.36 the flux escaping the storage formation. The attenuation is thus 64%. In Fig. 10 the fault permeability is 10× smaller (1 D) and the leakoff coefficient is also a factor of 10 smaller (-1.5×10^{-9} sec/m). The flux out the top of the fault now $-0.075/-0.21 \approx 0.36$ of the escape flux. Finally, in Fig. 11 we have again reduced the fault permeability and leakoff coefficient by a factor or 10 each and the attenuation into the permeable layer remains 64%.

In the next set of simulations we examine the effect of permeability variation within the fault. In these simulations the fault and fluid properties are largely the same as in the previous simulations. We assume one lateral leakage pathway exists along the fault between 1700-1750 m. Different values of the leakoff coefficient are chosen, from -1.5×10^{-8} sec/m to -1.5×10^{-11} sec/m. Figure 12 gives the mass flux along the fault with fault permeability fixed at 1 D (blue curve) and the mass flux when the fault permeability is 1 D except between 1400 (4590) and 1500 m (4920 ft) where it is taken to be very small (i.e., 0.0001 D) (magenta curve). We refer to this section of the fault as a choke point. In this simulation the leak has value -1.5×10^{-8} sec/m (i.e., a big leak). Figure 13 shows the final pore pressure at the end of simulation in red and hydrostatic pressure in blue. Figures 14 and 15 give the mass flux when the leakoff coefficient is one and two orders of magnitude smaller respectively (i.e., -1.5×10^{-9} sec/m and -1.5×10^{-10} sec/m). And finally, Fig. 16 gives the mass flux when the leakoff coefficient is smaller still (-1.5×10^{-11} sec/m). The gap between the constant and variable permeability curves widens, and the influence of the choke point becomes greater, as the leakoff coefficient becomes smaller. The attentuation into the permeable layer is close to 100% if the fault has a choke point above the layer.

Clearly if one is doing inventory on CO_2 in the storage formation, these results suggest that one could not tell just from the rate of escape whether the CO_2 is going into a harmless formation or rising up to the shallower subsurface. As was the case with the depth of the leakage layer, large fluxes of CO_2 can escape the storage formation without reaching the top of the fault, and on the other hand, relatively small fluxes may escape and undergo minimal attenuation, resulting in significant flux at the top of the fault. Our conclusion is, therefore, that *the leakage layer permeability (or leakoff coefficient) and the fault permeability distribution together dictate where leakage will occur. For large leakage layer permeability (i.e., $q_{leak} = 1\times10^{-8}$ sec/m), escape from the storage formation is almost independent of whether choke exists. For very small leakage layer permeabilty, the fault permeability dictates escape rate.* However, whether the fault has a choke point or not, the escape flux does not vary linearly with leakage layer permeability.

While layer dip angle γ does not appear to affect mass flux, the angle θ of fault inclination away from vertical does have some impact. In Fig. 17 we see three mass flux plots. In all cases there is a single leak from 1700-1750 m (5580-5740 ft) depth with leakoff coefficient of -1.5×10^{-11} sec/m. The fault permeability is constant at 1 D. All other parameters are as in previous simulations. The blue curve corresponds to a vertical fault. The magenta and red curves correspond to fault inclined at 45 and 60 degree angles from the vertical respectively. Buoyancy has less effect on attenuation in the inclined faults than in the vertical fault. Finally in Fig. 18 we show results from an identical simulation except that the over-pressurization at the bottom of the fault is taken to be 10× smaller, i.e., X = 0.5 MPa (72.5 psi) rather than X = 5 MPa (725psi). This change corresponds to a thinner CO_2 storage formation. We see negligible attenuation into the horizontal layer when we reduce the overpressure. Moreover, though the driving force is reduced by 10×, the flux escaping from the storage reservoir only changes by a factor of 2.

2D Modeling Approach

Overview. We develop a 2D model to test the assumptions in the quasi-1D model. Figure 19 describes the base case, which accounts for two fluid phases and a homogeneous storage formation at a depth of 1615 m (5300 ft). Initially the storage formation, surrounded by an impermeable formation, is saturated fully with CO_2 (S_g = 1.0). The intersection with a conductive fault on the top seal of the CO_2 reservoir allows leakage along the fault. To simulate geometric and petrophysical properties of a fault we set transmissibility multipliers on a series of grid blocks assigned to have fault characteristics. The fault is assigned isotropic permeability (k_v/k_h=1), while the matrix and the permeable layer(s) have anisotropic permeability (k_v/k_h<1). The storage formation is set at higher initial pressure (3.45 MPa or 500 psi more) than the surrounding formation. This is intended to account for the larger pressure during CO_2 injection and for the smaller pressure gradient (5.61 kPa/m or 0.248 psi/ft) in the CO_2 column. Outside the storage reservoir, the pressure gradient is taken to be hydrostatic (9.79 kPa/m or 0.433 psi/ft). Production wells at side boundaries are held at hydrostatic pressure. In effect, these wells establish an open boundary that does not perturb the pressure field. The worst-case leakage condition is that pressure at the bottom of the fault does not decrease. Thus we placed injection wells within the storage formation to replace CO_2 that escapes along the fault, thereby maintaining constant pressure within the storage formation (22.06 MPa or 3200 psi). We assume the whole domain is isothermal. To compare with the quasi-1D model, we place a constant-bottomhole-pressure producer (set to hydrostatic pressure) in the grid block at the top of the fault.

We compare the rates of escape from the storage formation and the rate of attenuation from quasi-1D and 2D simulation results. To do so, the leakoff coefficient in the quasi-1D model is computed directly from Eq. 9. For this calculation the density and viscosity of CO_2 are taken at the initial conditions in the storage compartment. The rates of escape and attenuation must be derived from the 2D simulation output. To do so, the values of CO_2 phase velocity and density at appropriate grid blocks are extracted from the output files. The CO_2 mass flux is the product of phase velocity and density; we neglect the mass of water dissolved in the CO_2 phase.

We then examine the effect of two-phase composition and geometric properties on the leakoff coeffcient. The goal here is to ensure that the simple estimate of Eq. 9 does not neglect any essential phenomena. We conduct 2D simulations with different values of permeability, thickness and dip angle of the permeable layer and the relative permeability curve for matrix rocks. The leakoff coefficient is derived from simulation output. The mass flux of CO_2 into the permeable layer is computed from the CO_2 phase density and velocity in a layer grid block adjacent to the fault grid block. The potential difference between the fault/layer intersection and the domain boundary, Eq. 7, is also extracted from the output. As shown in Eq. 8, the ratio of these quantities, $u\rho/\Delta\Psi$, is the apparent leakoff coefficient, i.e. the value of q_{leak} that should enable the quasi-1D model to reproduce the 2D results.

Comparison of Quasi-1D and 2D Results. Table 2 summarizes the properties of the test case. The 2D model, Fig. 19, was set up to mimic the assumptions of the quasi-1D model (hydrostatic pressure in the layers outside the fault, constant pressure at bottom and top of fault, distance L between fault and far-field boundary fixed by the positioning of constant-pressure wells at the domain boundary). The 2D model further assumes that the matrix other than the leakage layer has small permeability, so it does not affect the behavior. For convenience a vertical fault and horizontal permeable layer were assumed. (A dipping layer turns out to add a degree of complexity, discussed below.) The discretization was different in the two models, with 1 m spacing in the 1D model and $0.61\text{m(W)}\times0.61\text{m(L)}\times3.05\text{m(H)}$ (2 ft × 2 ft × 10 ft) elements in the 2D simulation. Thus the permeable layer was represented by a single grid block in the vertical direction. Subsequently we refined the grid in the vertical direction to 0.61 m (2 ft); the results are presented below.

As Fig. 20 and Table 3 show, the quasi-1D, single phase flow model and the 2D, full-physics model have the same trend of CO_2 fluxes. The rate of CO_2 escape from the storage formation is essentially the same for both models, 0.095 kg/m^2-s in 1D and 0.099 kg/m^2-s in 2D when the leakage layer has 1 darcy permeability. The 1D model correctly captures the nonlinear change in escape flux when the permeability of the leakage layer is changed: a ten-fold reduction in layer permeability reduces the escape flux only about 10%. The attenuation predicted by the 1D model, 46% of the escape flux for a 1 darcy leakage layer, is less accurate; the full-physics code indicates a 68% attenuation. However, the 1D model does stimate the nonlinear change in attenuation with layer permeability reasonably well. A ten-fold reduction in layer permeability reduces attenuation by a factor of six in the 1D model and by a factor of 4.5 in the 2D model.

We conclude that the 1D model captures the basic physics of the escape/attenuation process for short to moderately long faults. One qualification to this assertion is that the parameter L is well defined in the 2D simulation. For a fault intersecting an unbounded aquifer, a procedure to identify the appropriate value of L to enter into Eq. 9 needs to be developed.

Factors Controlling Leakoff Coefficient. As defined in Eq. 9, the leakoff coefficient will be determined by four parameters: CO_2 density and viscosity, subsurface permeability and a distance from the fault to the hydrostatic boundary of the layer. Here we examine the sensitivity of the behavior to these factors in full 2D simulations in order to validate our method of estimating q_{leak}, i.e. Eq. 9. Every case is based on two-phase flow and homogeneous reservoir as our 2D base model does. Also, the vertical fault has 9.87×10^{-13} m^2 (1 Darcy) of permeability.

Layer Properties (Permeability, Thickness & Dip Angle). The layer permeability is one of the main factors which determine the attenuation rate of CO_2 flowing in a fault. On the other hand the geometric properties of layer such as thickness (cross-sectional area) and dip angle should not influence leakoff coefficient. Table 4 shows that leakoff coefficients remain constant in spite of layer thickness variation while they vary proportionally according to layer permeability. This result is consistent with our analytic formula.

Table 5 show that the leakoff coefficient does depend on dip angle. Tilting the layer by 14 degrees reduces the coefficient by a factor of two to three relative to the horizontal case. The dip also increases the sensitivity of the leakoff coefficient to the layer permeability slightly. Recall that in the 1D single-phase flow results we did not see this impact from the dip angle of the layer. Moreover the primary effect of dip angle should be accounted for in the potential difference term, Eq. 7, and the leakoff coefficient should be independent of dip angle.

To investigate these unexpected factors, we carried out a grid refinement study. With the two-phase, 2D model the dip results in counter-current flow within the layer. Only part of the layer accommodates CO_2 flux, while water moves in the remainder of the layer. Thus the leakoff coefficient could be correctly characterizing the conductivity of the layer for CO_2; the problem is that as far as CO_2 is concerned, the layer is in effect thinner than its nominal thickness. To account for this dip effect in the 1D model we could reduce the thickness of the interval where the leakoff coefficient is applied. A horizontal layer intersecting a fault at 1700-1750 m might be represented instead as a tilted layer intersecting a fault from 1700-1720 m.

Rock Property (Relative Permeability Data). Figure 21 shows the relative permeability curves used to test sensitivity. The CO_2 phase endpoint relative permeabilities were changed, while the shape of the curves and the endpoint saturations were kept the same. Changing the CO_2 relative permeability by a factor of three has only a slight effect on the observed leakoff coefficient (Table 6). This is not obvious; it happens because CO_2 establishes a front with a characteristic saturation as it rises, analogous to the Buckley-Leverett front saturation (Lakshminarasimhan *et al*. 2006). The value of the frontal saturation in turn determines the relative permeability characterizing the CO_2/brine displacement (Kumar *et al*. 2008). Decreasing the CO_2 phase relative permeability increases this frontal saturation (Fig. 22). Consequently, the relative permeability that is characteristic of the CO_2 leaking into the layer is larger. The net result is that the leakoff coefficient is relatively insensitive to changes in the relative permeability.

Countercurrent Flow in Permeable Layer. We examine the behavior in dipping leakage layers more closely. The 2D full physics simulations show that less CO_2 enters a dipping layer than the 1D model predicts, but the models agree for horizontal layers. Fig. 23 shows how refined grids compose the permeable strata. The coordinate of a grid consists of two parts: the first one indicates mother grid and the later one defines finer grids.

Figure 23 shows CO_2 occupying the upper three or four sublayers of the leakage layer. The CO_2 saturation in the bottom sublayer is much smaller. The CO_2 has invaded less into the downdip zone due to its buoyancy. As shown in Fig. 24, larger dip amplifies the CO_2 override in the downdip direction. As a result, downdip leakoff coefficient decreases as dip angle increases.

Figure 25 introduces the CO_2 phase velocities overlaid on the CO_2 saturation profile. The velocity vectors distribute exactly the same way as we define three typical behaviors: CO_2 escapes from storage, attenuated CO_2 enters the permeable layer, and CO_2 leaks past layer. Figure 26 shows the water velocity distribution overlaid on CO_2 saturation. Brine inside the permeable strata is displaced by CO_2 entering the strata. But brine also sinks (slowly) in the updip part of the layer, occupying the bottom sublayer.

The modified leakoff coefficient obtained from these refined grid simulations is more consistent with the expectation from Eq. 9, though some dependence on dip angle persists (Table 7). We remark that the 1D model is necessarily symmetric with regard to the leakage layer; it cannot account for different behavior in the downdip and updip sides of the layer.

Conclusion

Leakage of CO_2 along a conductive fault that intersects a deep saline aquifer in which the CO_2 is stored can be treated with a quasi-1D “leaky conduit” model. We present a highly simplified version of this model suitable for incorporation in a risk assessment framework. The idealizations capture some of the essential physics and thereby provide insight on important couplings within the system. The model is an attempt to enable assessments of leakage fluxes when the flow properties of formations and faults intersecting them are poorly constrained.

The analytical leakoff coefficient approach assumes 1D, single phase and slightly compressible flow. The leakoff coefficient based on Darcy's law consists of five characteristic parameters: density and viscosity of CO_2, relative permeability, absolute permeability of the layer, and the distance from attenuation point to hydrostatic boundary. Full-physics simulations in 2D indicate that this simple estimate is reasonable, and that the quasi-1D model captures key features of CO_2 migration in faults over moderate distances (< 1 km). The assumption of slight compressibility is the main limitation on applicability to longer distances.

The results from the quasi-1D model study show that the location of permeable layer(s) plays a significant role in determining the rate of attenuation of the rising CO_2 flux. Deeper layers provide much more attenuation than shallower layers. Ironically, more CO_2 escapes from the storage formation, but less CO_2 reaches the top of the fault, if the leakage layer is deeper. This nonlinearity is exacerbated if the fault has a low permeability section above the leakage layer. Thus attenuation can reduce risk associated with CO_2 reaching the top of the fault, even if more CO_2 leaves the storage formation. Attenuation is proportional to the ratio of fault permeability to leakoff coefficient. The interaction between CO_2 and water phases complicates attenuation behavior in the dipping layer. Denser fluid (brine) will occupy the lower part of a permeable zone depending on the dip angle. Consequently, applying the leakoff coefficient to the entire thickness of the layer will overestimate the attenuation.

Acknowledgements

We thank the sponsors of the Geologic CO_2 Storage Joint Industry Project at the University of Texas at Austin: BP, Chevron, CMG, ConocoPhillips, ExxonMobil, Luminant and Shell.

Nomenclature

A = cross-sectional area of layer, ft^2 or m^2
c_f = fluid compressibility, psi^{-1} or Pa^{-1}
c_r = rock compressibility, psi^{-1} or Pa^{-1}
D = depth vector
F_i = driving force on refined layer i, lb/ft sec^2 or kg/m sec^2 (i = layer index)
g = gravitational acceleration, ft/sec^2 or m/sec^2
k_{layer} = absolute permeability of layer, md or m^2
L = distance between fault and hydrostatic boundary, ft or m
p = pressure, psi or Pa
q = flow rate, ft^3/sec or m^3/sec
q_{leak} = leakoff coefficient, sec/ft or sec/m
$q_{leak,i}$ = leakoff coefficient for refined i^{th} layer, sec/ft or sec/m
$q_{leak,total}$ = total leakoff coefficient (summation of $q_{leak,i}$), sec/ft or sec/m
r_i = radial distance for boundary i, ft or m
z = depth, ft or m
φ = mass flux, lb/ft^2sec or kg/m^2sec
$\varphi_{\text{Attenuation}}$ = mass flux of attenuated CO_2 leaks, lb/ft^2sec or kg/m^2sec
φ_i = mass flux for refined layer i, lb/ft^2sec or kg/m^2sec
μ_{CO_2} = viscosity of carbon dioxide, cp or Pa-s
γ = dip angle of layer, degree
θ = inclination angle of fault, degree
ρ_{CO_2} = density of carbon dioxide, lb/ft^3 or kg/m^3
Ψ = potential

Reference

Bachu, S., Gunter, W.D. and Perkins, E.H., "Aquifer Disposal of CO_2 - Hydrodynamic and mineral trapping," Energy Convers Manage, 35(4):269-279, 1994

Chang, K.W. and Bryant, S.L., "Dynamics of CO_2 Plumes Encountering a Fault in a Reservoir," 6th Annual Conference on Carbon Capture and Sequestration, DOE/NETL, Pittsburgh, PA, May 7-10, 2007

Chen, Z., Huan, G., Ma, Y., "Computational Methods for Multiphase Flows in Porous Media," Society for Industrial and Applied Mathematics, Philadelphia, PA, 2006

Ewing, R., "Problems arising in the modeling of processes for hydrocarbon recovery. In: Ewing, R.E. (Ed.)," The Mathematics of Reservoir Simulation. SIAM, Philadelphia, PA, pp. 35-106, 1983

Huerta, N.J., Conrad, L and Bryant, S.L., "Cement Core Experiments With A Conductive Leakage Pathway, Under Confining Stress And Alteration Of Cement's Mechanical Properties Via A Reactive Fluid, As An Analog For CO_2 Leakage Scenario," SPE 113375 presented at SPE Improved Oil Recovery Symposium, Tulsa, OK, April 19-23, 2008

Intergovernmental Panel on Climate Change (IPCC), "Special Report on Carbon Dioxide Capture and Storage," pp 196-276, downloaded April 2007 from http://www.ipcc.ch/ipccreports/special-reports.htm, 2006

Kumar, N., "CO_2 Sequestration: Understanding the Plume Dynamics and Estimating Risk," Master Thesis, Univ. of Texas at Austin, 2008

Lakshminarasimhan, S., Bryant, S.L. and Pope, G.A., "Buoyancy-Dominated Multiphase Flow and its Impact on Geological Sequestration of CO_2," SPE 99938 presented at SPE/DOE Improved Oil Recovery Symposium, Tulsa, OK, April 22-26, 2006

Lindeberg, E., "Escape of CO_2 from aquifers," Energy Convers Manage. 38(Suppl.):S235-S240, 1997

Noh, M. Lake, L., Bryant, S.L. and Araque-Martinez, A. 2007. Implications of Coupling Fractional Flow and Geochemistry for CO2 Injection in Aquifers, *SPEREE* **10** (4): 406-411.

Nghiem, L., Sammon, P., Grabenstetter, J. and Ohkuma, H., "Modeling CO_2 Storage in Aquifers with a Fully-coupled Geochemical EOS Compositional Simulator," SPE 89474 presented at SPE/DOE Improved Oil Recovery Symposium, Tulsa, OK, April 22-26, 2006

Oldenburg, C.M. and Unger, A.J., "On Leakage and Seepage from Geologic Carbon Sequestration Sites: Unsaturated Zone Attenuation," Soil Science Society of America, Vadose Zone Journal, 2:287-296, 2003

Oldenburg, C.M., Bryant, S.L., and Nicot, J.-P., "Certification framework based on effective trapping to meet the unprecedented challenges of geologic CO_2 storage (abs.)," *in* 2008 UIC Conference: What's hot in UIC!, Ground Water Protection Council, New Orleans, January 14-16, 2008

Oldenburg, C.M. and Bryant, S.L., "Certification Framework for Geologic CO2 Storage," National Energy Technology Laboratory 6th Annual Conference on Carbon Capture and Sequestration, Pittsburgh, PA, 7-10 May 2007

Pruess, K., "Numerical Simulation of CO_2 Leakage from a geologic Disposal Reservoir Including Transitions from Super- to Sub-critical Conditions, and Boiling for Liquid of CO_2," LBNL 52423, Lawrence Berkeley National Laboratory, 2003

Saadatpoor, E., Bryant, S.L. and Sepehrnoori, K., "Effect of Heterogeneous Capillary Pressure on Buoyancy-driven CO_2 Migration," SPE 113984 presented at SPE Improved Oil Recovery Symposium, Tulsa, OK, April 19-23, 2008

Yielding, G., Freeman, B. and Needham, D.T., "Quantitative Fault Seal Prediction," American Association of Petroleum Geologists Bulletin; Vol. 81; No. 6; pp. 897-917, June 1997

Table 1—Carbon dioxide compressibility values for the slightly compressible model of CO_2 density, Eq. 5. In our simulation works, we consider only "deep leak."

Region	Range of depths	c_f, Pa^{-1}
"shallow leak"	$0 < z < 600$ m	1.66×10^{-7}
"deep leak"	1100 m < z	1.82×10^{-8}

Table 2—Description of model properties and parameters for analytical leakoff coefficient; both quasi-1D and 2D models involves the same properties of reservoir and structures.

Property		Value
Location	Fault	In the middle of reservoir
	Layer	5800 ft (below the earth)
Permeability	Fault	9.87×10^{-13} m^2
	Layer	9.87×10^{-13} or 10^{-14} m^2
Pressure gradient		9.79 kPa/m
Compressibility		1.82×10^{-8} Pa^{-1}
1D Leakoff coefficient	1000 md Layer	5.24×10^{-9} sec/m
	100 md Layer	5.24×10^{-10} sec/m
Parameters for 2D Analytical Leakoff Coefficient	Relative Permeability (k_r)	0.157
	Density (ρ_{CO2})	643.30 kg/m^3
	Viscosity (μ_{CO2})	6.81×10^{-5} Pa-s
	Distance (L)	304.8 m

Table 3—Comparison of CO_2 escape flux from storage formation and attenuation into a single permeable layer from quasi-1D and 2D simulation outputs (assuming the same reservoir properties).

Layer permeability, m^2		Escape Rate from Storage, kg/m^2s	Attenuation, %
9.87×10^{-13}	1D	9.18×10^{-2}	46
	2D	10.00×10^{-2}	68
9.87×10^{-14}	1D	8.20×10^{-2}	8
	2D	8.49×10^{-2}	15

Table 4—Comparison of leakoff coefficients from a series of simulation results; the variable parameters are thickness and absolute permeability of the layer. Leakoff coefficients are consistent to the variation of layer permeability, while they are not affected by the variation of layer thickness. This result validates our simple analytical approach of leakoff coefficient.

Layer Permeability, m^2	Layer Thickness, m	Leakoff Coefficient, sec/m
9.87×10^{-13}	3.05	5.24×10^{-9}
	9.14	4.92×10^{-9}
	15.24	4.95×10^{-9}
Analytical Solution		4.79×10^{-9}
9.87×10^{-14}	3.05	5.12×10^{-10}
	9.14	5.18×10^{-10}
	15.24	5.05×10^{-10}
Analytical Solution		4.79×10^{-10}
9.87×10^{-15}	3.05	5.15×10^{-11}
	9.14	5.05×10^{-11}
	15.24	4.92×10^{-11}
Analytical Solution		4.79×10^{-11}

Table 5—Comparison of leakoff coefficients from a series of simulation outputs; The variable parameters are dip/non-dip, dipping status and layer permeability (assuming dip angle is constant, 14°). For horizontal layer leakoff coefficient is proportional to layer permeability, while for tilted layer leakoff coefficient varies according to dipping status. The dipping condition causes inconsistency of analytical estimation of leakoff coefficient due to the interaction between brine and CO_2 phases.

Layer Permeability, m^2	Layer Geometry		Leakoff Coefficient, sec/m
9.87×10^{-13}	Horizontal		5.24×10^{-9}
	Tilted	Downdip	3.18×10^{-9}
		Updip	1.74×10^{-9}
9.87×10^{-14}	Horizontal		5.12×10^{-10}
	Tilted	Downdip	2.79×10^{-10}
		Updip	1.93×10^{-10}
9.87×10^{-15}	Horizontal		5.15×10^{-11}
	Tilted	Downdip	1.57×10^{-11}
		Updip	2.89×10^{-11}

Table 6—Comparison of leakoff coefficients; the variable parameter is relative permeability data. This table shows the leakoff coefficient is affected by relative permeability curve.

Relative Permeability	Layer Permeability, m^2	Leakoff Coefficient, sec/m	
		Simulation	Analytical
BASE	9.87×10^{-13}	4.85×10^{-9}	4.79×10^{-9}
	9.87×10^{-14}	4.82×10^{-10}	4.79×10^{-10}
	9.87×10^{-15}	5.05×10^{-11}	4.79×10^{-11}
BASE ÷ 2	9.87×10^{-13}	4.20×10^{-9}	3.74×10^{-9}
	9.87×10^{-14}	4.39×10^{-10}	$3.74v10^{-10}$
	9.87×10^{-15}	4.49×10^{-11}	3.74×10^{-11}
BASE ÷ 3	9.87×10^{-13}	3.97×10^{-9}	3.05×10^{-9}
	9.87×10^{-14}	3.87×10^{-10}	3.05×10^{-10}
	9.87×10^{-15}	4.23×10^{-11}	3.05×10^{-11}

Table 7—Comparison of leakoff coefficient from simulation outputs using refined grid blocks and analytical estimation using mass flux derivation. The variable partaker is dip angle of layer. The leakoff coefficient derivation using refined griding will be reasonable to estimate CO_2 leaks and its attenuation. This table also shows leakoff coefficients vary corresponding to layer dip and dipping status (updip & downdip). As we expected from simulation outputs, downdip leakoff coefficient decreases as dip angle increase.

Refined Grids System			Leakoff Coefficient, sec/m
Analytical Solution			2.39×10^{-9}
Simulation Horizontal Case			2.46×10^{-9}
Simulation Tilted Case	14°	Downdip	3.02×10^{-9}
		Updip	2.10×10^{-9}
	19°	Downdip	1.31×10^{-9}
		Updip	1.97×10^{-9}

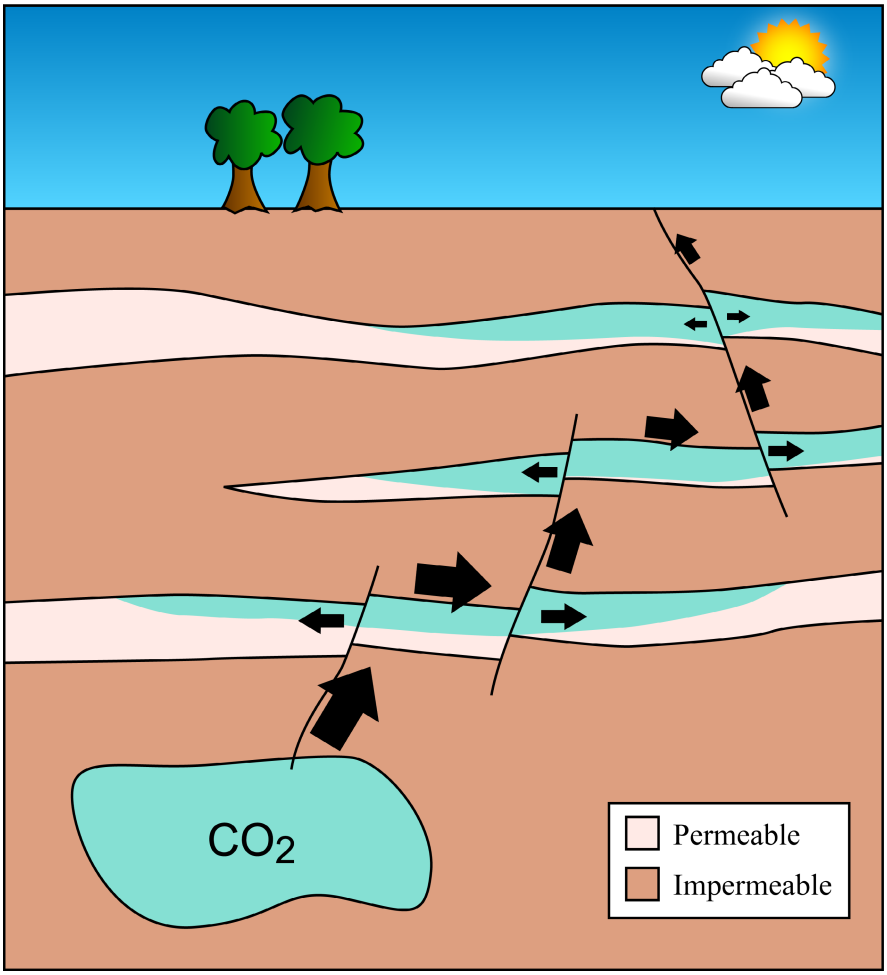

Fig. 1—Conceptual illustration for risks of underground CO_2 leakage along faults. Our model focuses on the fault zone encountering permeable layer(s). Injected CO_2 migrates and meets a conductive fault. The combination of fluid pressure and buoyancy drives CO_2 up the fault. The presence of permeable layer(s) attenuates the upward flux of CO_2. Continued leakage from fault into permeable layers can lead to encounter with another fault, and the process of upward migration and attenuation into permeable layers continues.

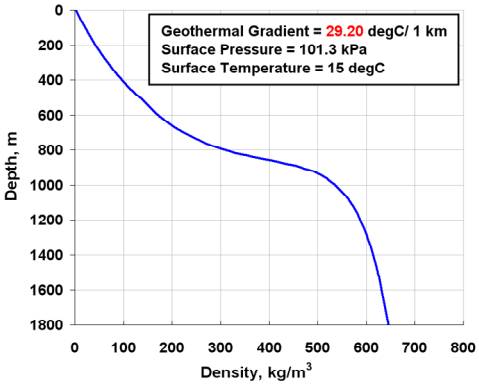

(a)

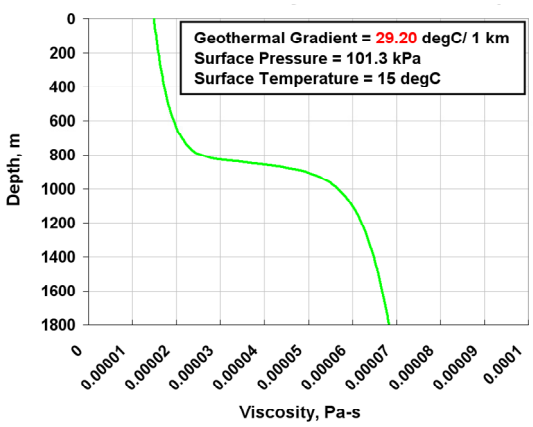

(b)

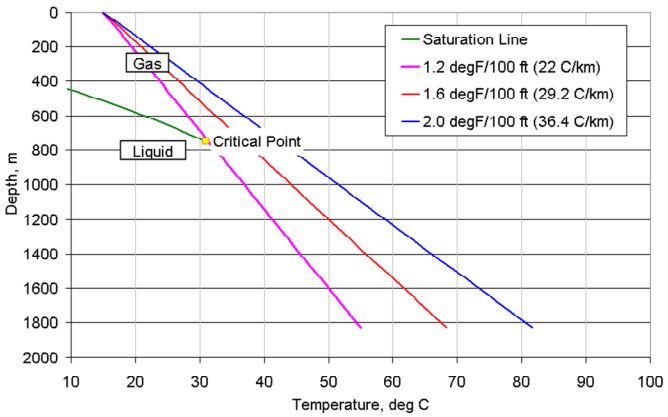

(c)

Fig. 2—(a) Density of pure CO_2 varies almost linearly with depth for depths greater than about 1200 m, assuming a constant hydrostatic pressure gradient and geothermal gradient. Values used in this plot are 9.79 kPa/m for pressure gradient and 29.20°C/km for geothermal gradient with surface conditions of 101.3 kPa and 15°C. (b) For the same conditions as (a), the viscosity of the CO_2 phase does not vary greatly for depths below 1200 m. (c) For typical geothermal and hydrostatic gradients (surface conditions of 101.3 kPa and 15°C), and for all depths below 800 m, CO_2 exists as a single phase.

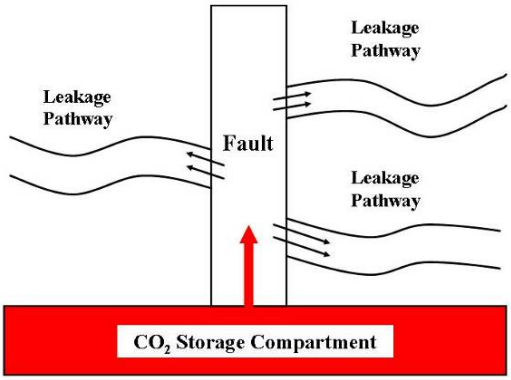

Fig. 3—Schematic illustration of fault leakage model. CO_2 plume escapes the storage formation through a conductive fault. It migrates up the fault. If the fault intersects permeable layer, the CO_2 can leak from the fault into the layer, resulting in attenuation of the escape flux.

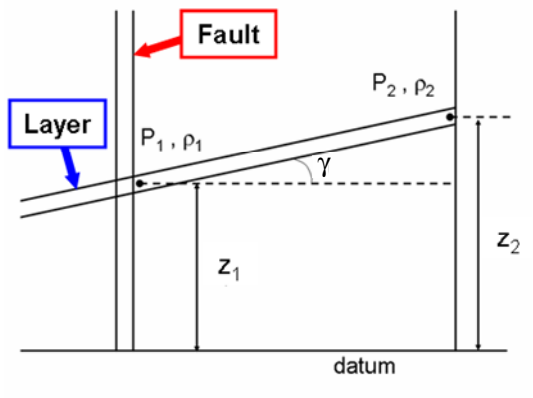

Fig. 4—Schematic illustration for potential derivation.

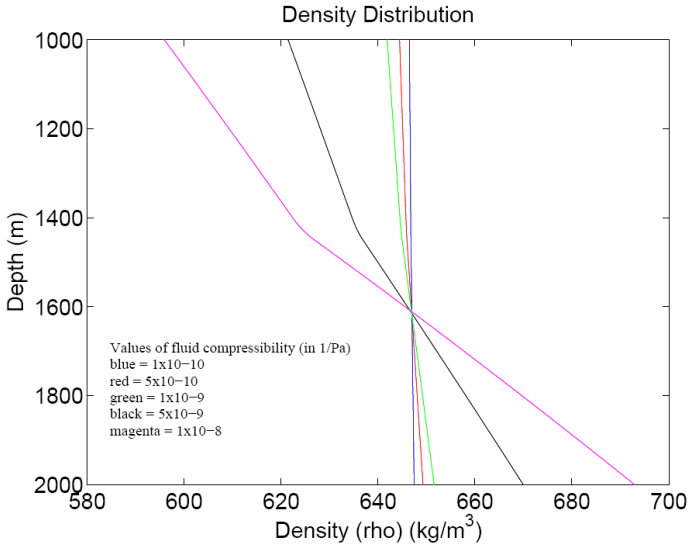

Fig. 5—Density of CO_2 along fault at steady state flow with different compressibility values used in Eq. 5. Simulation models a fault with a single leak between 1400-1450 m. Magenta curve: fluid compressibility = 1×10^{-8} Pa^{-1}; Black curve: $c_f = 5\times10^{-9}$ Pa^{-1}; Green curve: cf = 1×10^{-9} Pa^{-1}; Red curve: $c_f = 5\times10^{-10}$ Pa^{-1}; Blue curve: $c_f = 1\times10^{-10}$ Pa^{-1}.

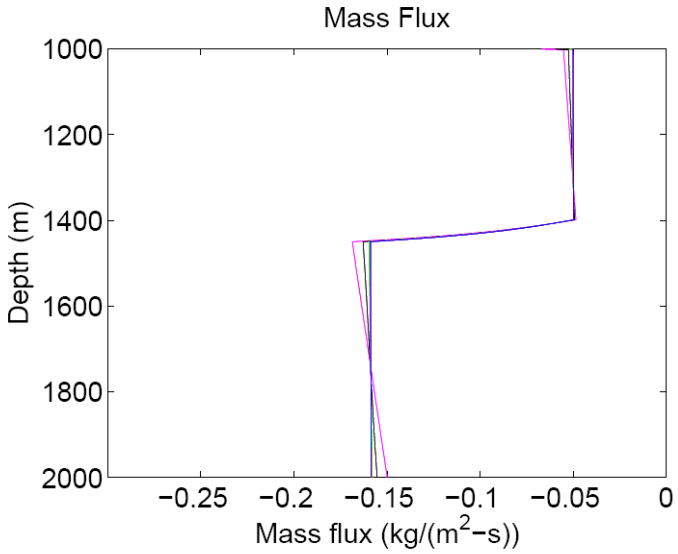

Fig. 6—Steady state mass flux along fault when fluid compressibility varies. In this simulation we consider a single leak between 1400-1450 m. Magenta curve: fluid compressibility = 1×10^{-8} Pa^{-1}; Black curve: $c_f = 5\times10^{-9}$ Pa^{-1}; Green curve: $c_f = 1\times10^{-9}$ Pa^{-1}; Red curve: $c_f = 5\times10^{-10}$ Pa^{-1}; Blue curve: $c_f = 1\times10^{-10}$ Pa^{-1}.

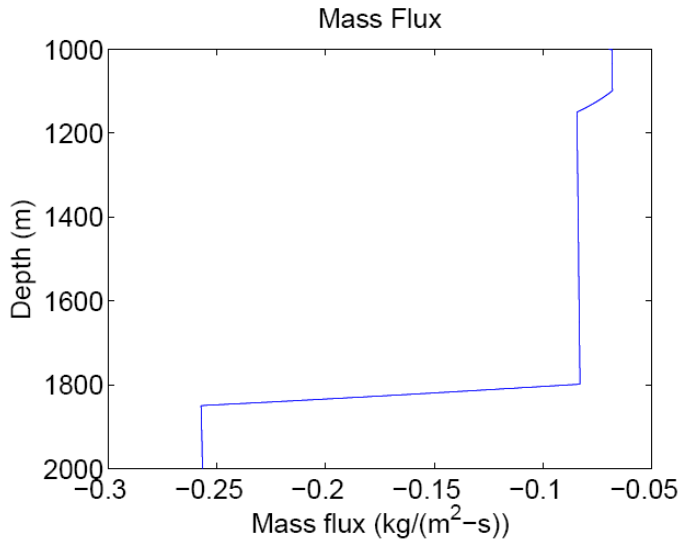

Fig. 7—Mass flux along fault for simulation with two identical permeable layers (same leakoff coefficients) at different depths. Fault permeability is uniform at 1 D. The leaks occur at 1100-1150 m and from 1800-1850 m depth. In these two intervals q_{leak} takes the value -1.5×10^{-9} sec/m.

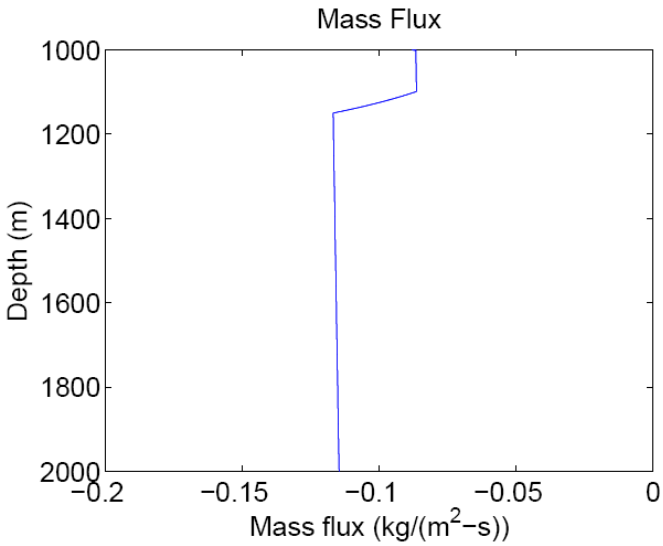

Fig. 8—Mass flux along fault for a simulation with a single shallow permeable layer at a depth of 1100-1150 m of size q_{leak} = -1.5×10^{-9} sec/m.

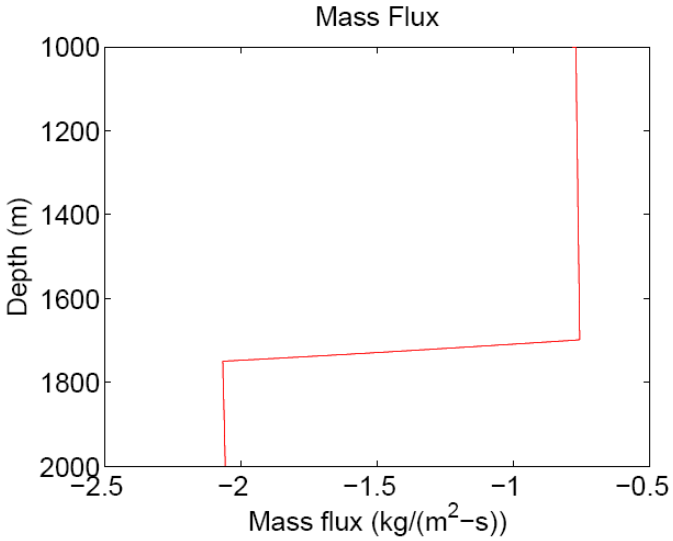

Fig. 9—Mass flux along fault for a simulation with a single permeable layer between 1700–1750 m depth with leakoff coefficient of -1.5×10^{-8} sec/m. The fault permeability is uniform at 10 D.

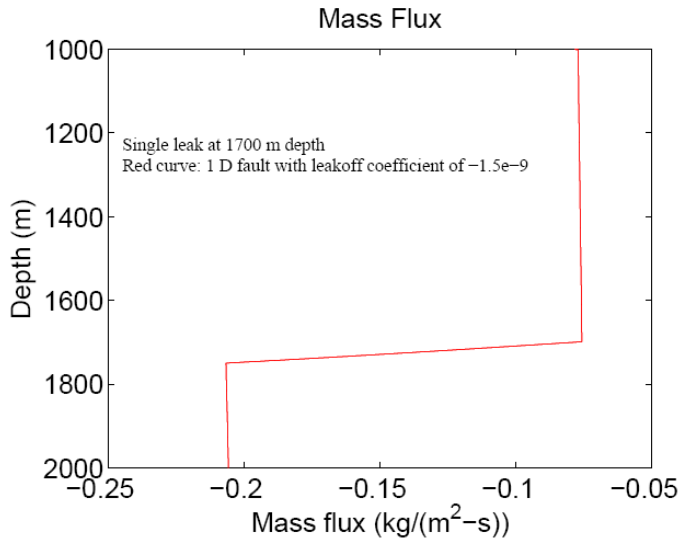

Fig. 10—Mass flux along fault for a simulation in which the fault permeability is 1 D and the leakoff coefficient is -1.5×10^{-9} sec/m.

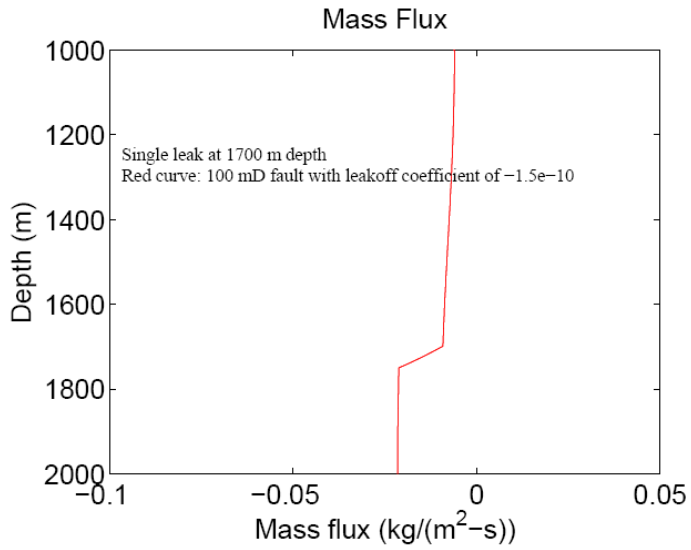

Fig. 11—Mass flux along fault for a simulation in which the fault permeability is 100 mD and the leakoff coefficient is -1.5×10^{-10} sec/m.

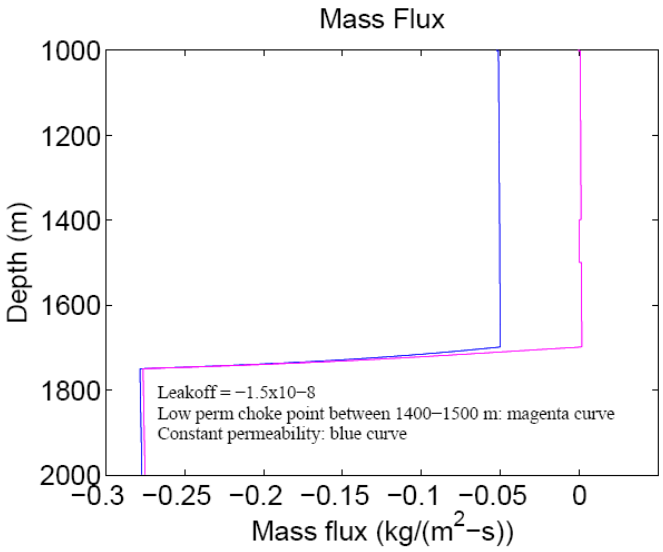

Fig. 12—Mass flux along fault for simulations with one permeable layer between 1700-1750 m. The leakoff coefficient is -1.5×10^{-8} sec/m (i.e., a big leak). Blue curve: mass flux with fault permeability fixed at 1D. Magenta curve: The fault permeability is 1 D except between 1400 and 1500 m where it is taken to be very small (i.e., 0.0001 D).

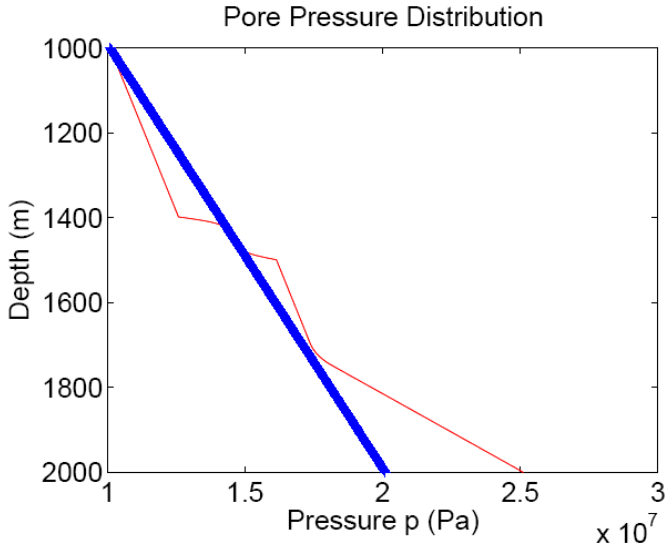

Fig. 13—Pore pressure at the end of simulation for the simulation described in Figure 12. One permeable layer is between 1700-1750 m. The leakoff coefficient is -1.5×10^{-8} sec/m with fault permeability fixed at 1 D except between 1400 and 1500 m where it is taken to be 0.0001 D. The red curve gives the final pore pressure at the end of simulation and the blue curve is hydrostatic pressure.

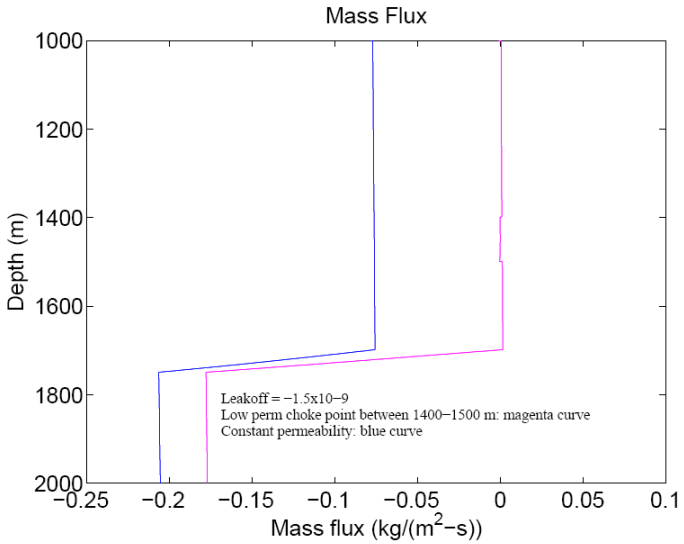

Fig. 14—Mass flux values for simulations with one leakage pathway between 1700-1750 m. The leak has value -1.5×10^{-9} sec/m. Blue curve: mass flux with fault permeability fixed at 1D. Magenta curve: mass flux when the fault permeability is 1D except between 1400 and 1500 m where it is taken to be very small (i.e., 0.0001D).

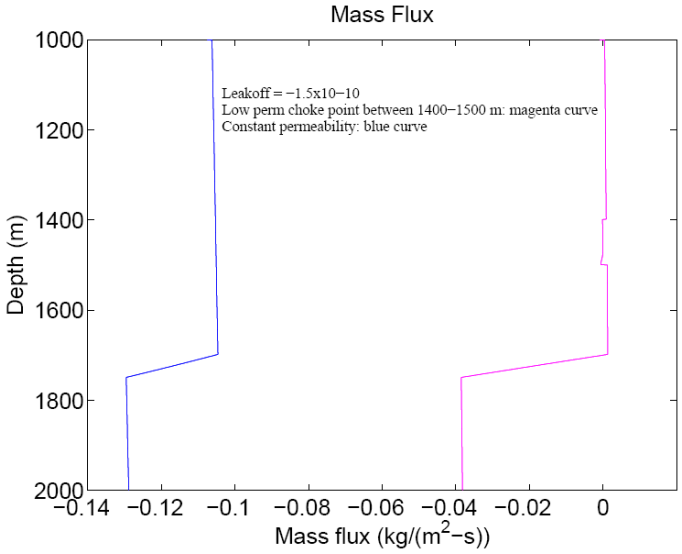

Fig. 15—Mass flux values for simulations with one leakage pathway between 1700-1750 m. The leak has value -1.5×10^{-10} sec/m. Blue curve: mass flux with fault permeability fixed at 1D. Magenta curve: mass flux when the fault permeability is 1D except between 1400 and 1500 m where it is taken to be very small (i.e., 0.0001D).

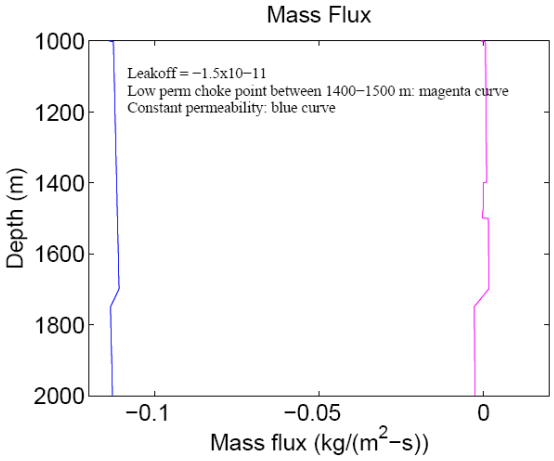

Fig. 16—Mass flux values for simulations with one leakage pathway between 1700-1750 m. The leak has value -1.5×10^{-11} sec/m. Blue curve: mass flux with fault permeability fixed at 1D. Magenta curve: mass flux when the fault permeability is 1D except between 1400 and 1500 m where it is taken to be very small (i.e., 0.0001 D).

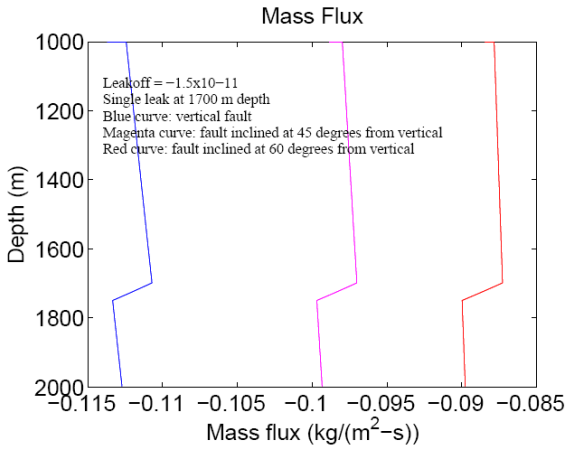

Fig. 17—Mass flux for simulations with a single leak from 1700-1750 m depth with leakoff coefficient of -1.5×10^{-11} sec/m. Constant fault permeability of 1D. Blue curve corresponds to a vertical fault. The magenta and red curves correspond to faults inclined at 45 and 60 degree angles from the vertical respectively. Here the overpressurization due to the CO_2 storage compartment is 5 MPa at the bottom of the fault.

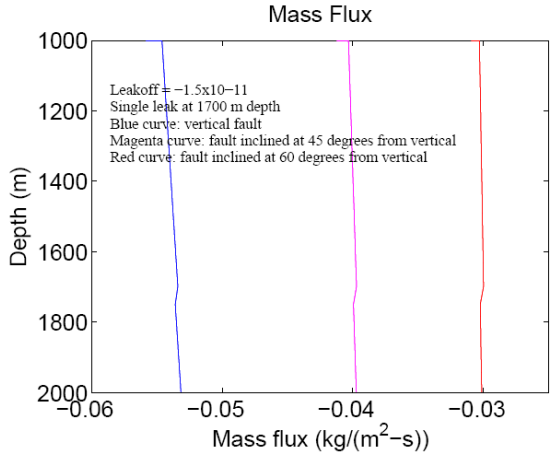

Fig. 18—Mass flux for simulations with a single leak from 1700-1750 m depth with leakoff coefficient of -1.5×10^{-11} sec/m. Constant fault permeability of 1D. Blue curve corresponds to a vertical fault. The magenta and red curves correspond to faults inclined at 45 and 60 degree angles from the vertical respectively. Here the overpressurization due to the CO_2 storage compartment is 0.5 MPa at the bottom of the fault.

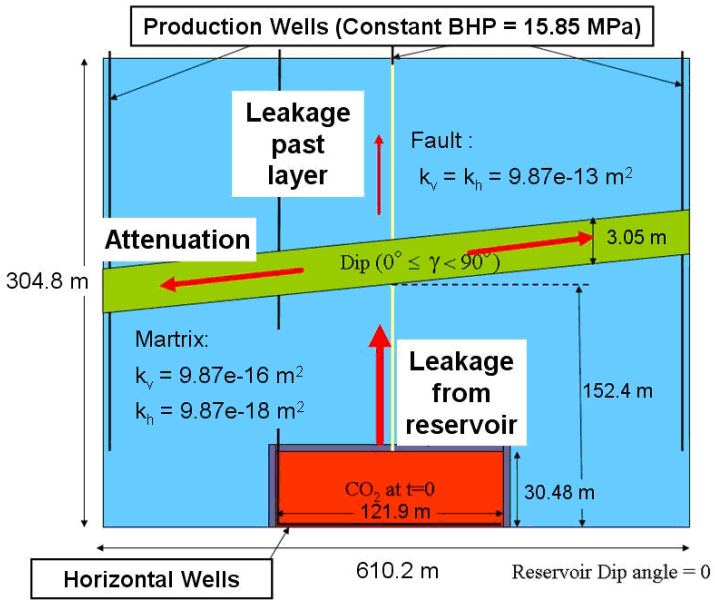

Fig. 19—Schematic description of 2D model assuming homogeneous reservoir with hydrostatic boundaries. The top of this model domain is located 1615 m (5300 ft) below the surface. The red lines represent CO_2 plume migration through permeable structures.

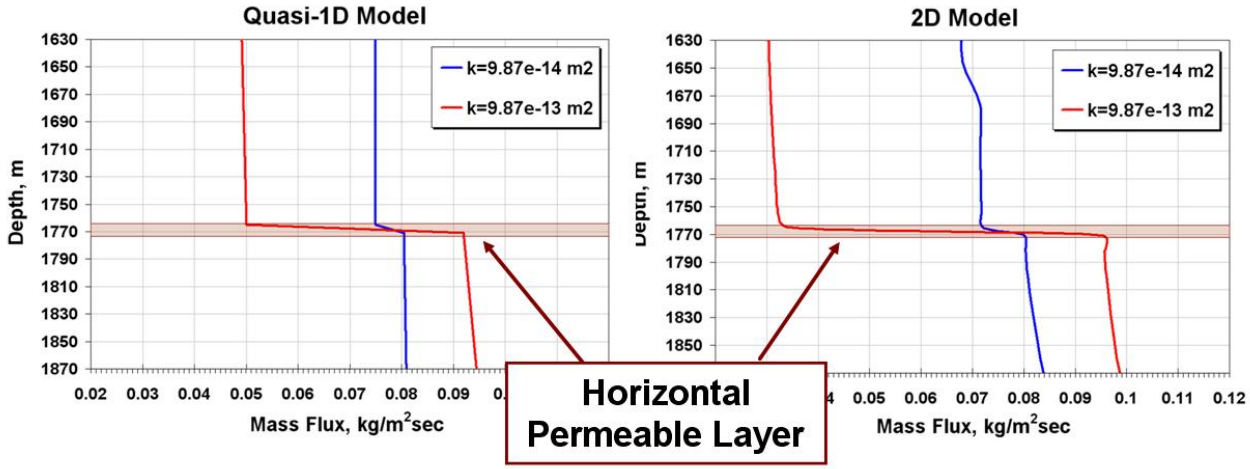

Fig. 20—Comparison of mass flux distribution from quasi-1D and 2D simulation outputs. Both show quite similar trend, initially CO_2 leaks happens and then the leak is attenuated into the permeable layer.

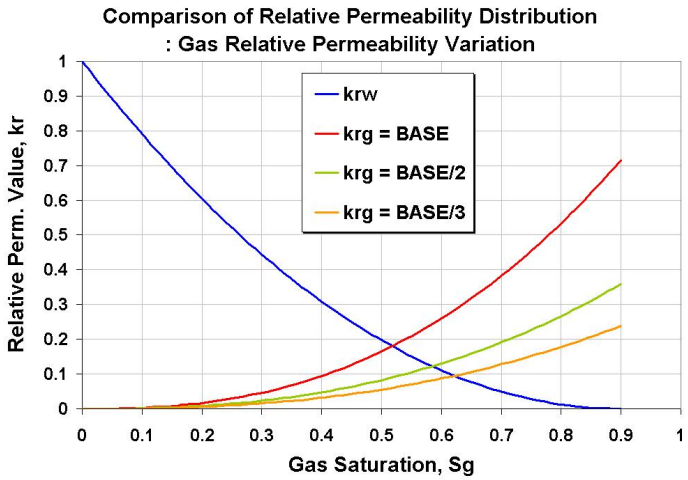

Fig. 21—Artificial relative permeability curve distribution; Only drainage curves for gas phase vary proportionally. Other values associated with hysteresis or water phase are fixed for this simulation study.

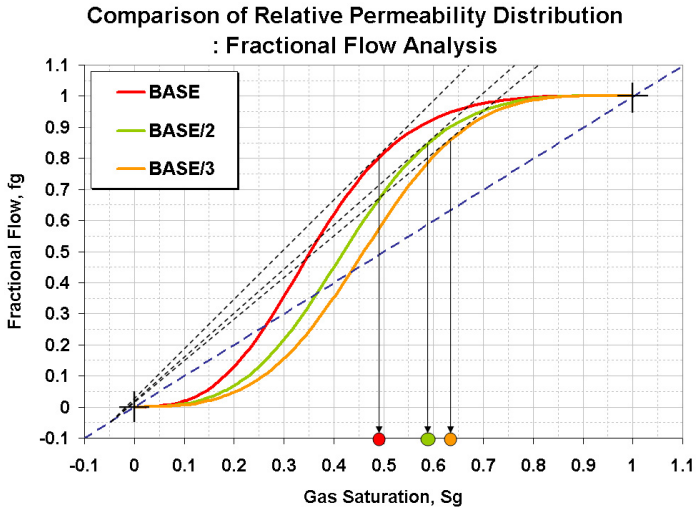

Fig. 22—Fractional Flow Curves with end-point saturation variation; Decreasing CO_2 phase saturation results in increasing its frontal saturation (Buckley-Leverett front). Then relative permeability of CO_2 plumes increases corresponding to given relative permeability curve.

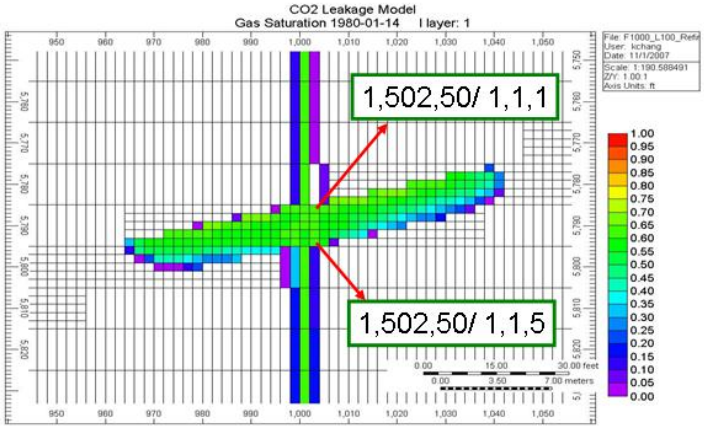

Fig. 23—Gas saturation profile of tilted model using refined grid blocks, which divide the layer into five separated layers. The coordinates in green boxes represent refined grid blocks. Mass fluxes for each layer are different, and the summation of them defines total mass flux of attenuated CO_2 inside the layer.

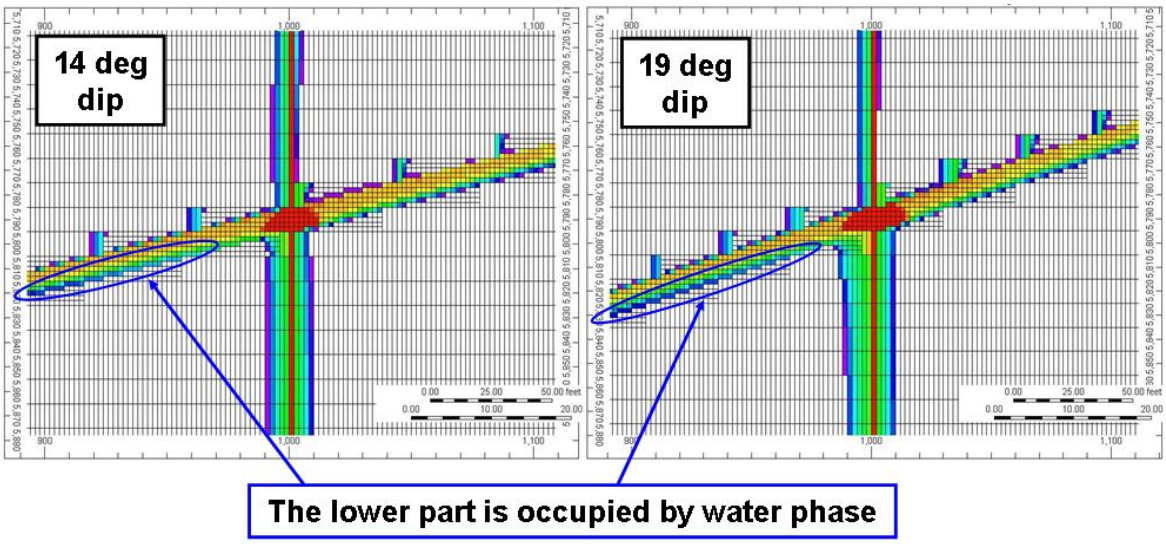

Fig. 24—Saturation profiles for comparison of layer dip angle variation. The downdip zone of more tilted layer is occupied more by brine phase. Thus, leakoff coefficient for downdip will be less than for updip.

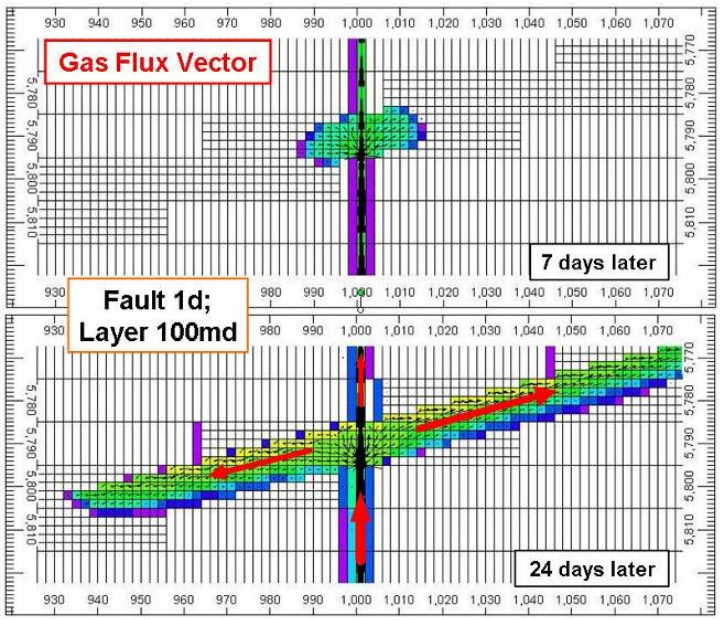

Fig. 25—Gas flux vector distribution superimposed on gas saturation profile. Larger flux of gas phase flows through updip.

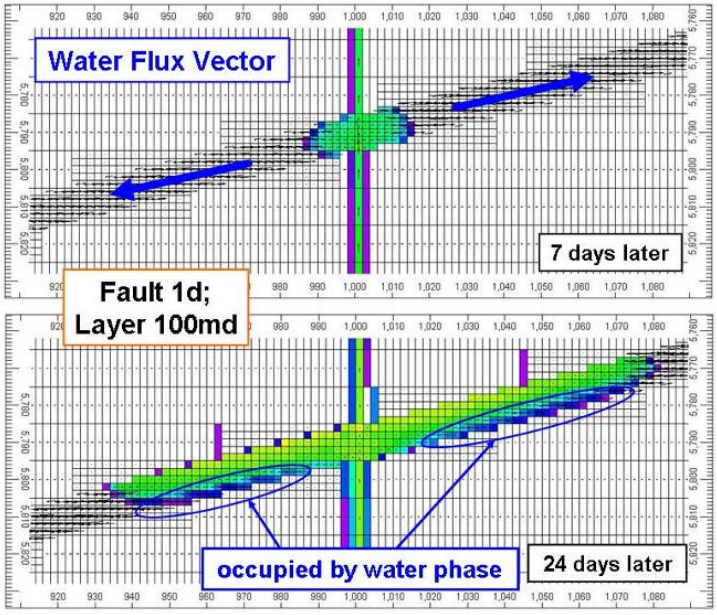

Fig. 26—Water flux vector distribution overlapped with gas saturation profile (tilted layer case, dip angle is 14°). In the upper figure, blue arrows represent that attenuated CO_2 pushes pre-occupied brine inside the layer. In the lower figure, the bottom part of the layer is occupied by brine, which means less dense fluids (CO_2) migrate through the upper part of the layer while denser fluids (brine) occupy the lower part. In addition, according to dipping status (updip and downdip) the region at which CO_2 migrates is different. Buoyant force make CO_2 migrate upward so that the updip zone of the layer is invaded by CO_2 rather than the downdip zone.